Development and testing of a snow interceptometer to quantify canopy interception in the rain/snow transition zone of the North Cascades, Washington, USA

Kael Martin

A thesis

submitted in partial fulfillment of the requirements for the degree of

Master of Civil and Environmental Engineering

University of Washington

2012

Committee:

Jessica Lundquist

Jeffery Berman

Program Authorized to Offer Degree:

Civil and Environmental Engineering

University of Washington

Abstract

Development and testing of a snow interceptometer to quantify canopy interception in the rain/snow transition zone of the North Cascades, Washington, USA

Kael A. Martin

Chair of the Supervisory Committee:
Dr. Jessica Lundquist
Civil and Environmental Engineering

Tree canopy snow interception is a significant hydrological process, capable of removing up to 60% of snow from the ground snowpack. Our understanding of canopy interception has been limited by our ability to measure whole canopy interception in an undisturbed forest setting. This study presents a relatively simple and inexpensive technique for directly measuring snow canopy interception using an interceptometer, adapted from *Friesen et al.* [2008]. Changes in canopy mass due to interception result in a measureable trunk compression, according to Hooke's law of elasticity. The interceptometer is composed of four linear motion position sensors distributed evenly around the tree trunk, which directly measure trunk displacement caused by interception. Through calibration techniques, the amount of canopy snow required to produce the measured displacements can be calculated. We incorporate a trunk laser-mapping installation method for precise sensor placement to reduce signal noise attributed to sensor misalignment. The simple design of the interceptometer allows for installation in relatively remote locations with limited vehicle and power access. Through interceptometer development and installation, we demonstrate instrument performance on a western hemlock (*Tsuga heterophylla*) for a snow interception event in late November, 2011. Our study finds a snow interception efficiency of 83 ±15% of total accumulated ground snowfall with a maximum interception capacity of 50 ±8 mm snow water equivalent (SWE). The observed interception event is compared to simulated

interception represented by the Variable Infiltration Capacity (VIC) hydrologic model. The model generally underreported interception magnitude by 33% using an LAI of 5 and 16% using an LAI of 10. The interceptometer was also able to capture periods of intrastorm accumulation of up to 3 mm SWE hr^{-1} and drip melt rates of 0.75 mm SWE hr^{-1}, which the model failed to represent. While further validation is necessary to reduce instrument error, our results indicate that forest interception magnitude may be underestimated in maritime areas such as the Pacific Northwest. Through further instrument development and deployment, this method may prove to be a valuable tool capable of providing direct canopy snow interception estimates within intact canopy structures at high temporal resolution and sensitivity.

TABLE OF CONTENTS

Page

List of Figures ……iii

List of Tables ……iv

Chapter 1: Introduction ……...……...1

Chapter 2: Theory and background ……5

Chapter 3: Methods ……7

3.1 Site description ……..7

3.2 Snow surveys ……8

3.3 Interceptometer installation ……..8

3.4 Interceptometer data collection ……...10

3.5 Potentiometer calibration ……10

3.6 Data processing to isolate compression signal ……11

3.6.1 Bending ratio method ……...11

3.6.2 Strain diagram method ……15

3.7 Modulus of elasticity ……...16

3.8 SWE calculations ……19

3.9 Modeling ……19

Chapter 4: Results ……21

Chapter 5: Discussion …… ……28

5.1 Interceptometer evaluation and sensitivity analysis ……...28

5.2 Interceptometer comparison to previous literature and model output ……29

5.3 Recommendations for future installation ……...32

5.4 Broader implications ……..33

Chapter 6: Conclusion ……...35

References ……36

Appendix A ……...40

LIST OF FIGURES

Figure Number Page

3.1 Site map, instrument orientation, and installed interceptometer ……...7

3.2 Bending test schematic ……...12

3.3 Bending ratio test ……14

3.4 Strain diagram conceptual map ……...16

3.5 Modulus of elasticity calibration ……18

4.1 Raw and processed snow event data ……...22

4.2 Snow interception computed ……...23

4.3 Efficiency of interception ……...24

4.4 Model comparison ……..25

4.5 Zoomed view during storm ……27

LIST OF TABLES

Table Number Page

5.1 Literature comparison ……31

ACKNOWLEDGEMENTS

This work was made possible through funding provided by NSF Grant No. CBET-O931780 to Jessica Lundquist of the University of Washington.

I would like to thank the members of my Master's Committee Jessica Lundquist and Jeffery Berman for continued research support, guidance, and inspiration.

I would also like to thank members of the Mountain Hydrology Research Group: Mark Raleigh, Brian Henn, Shara Feld, Nic Wayand, Nicoleta Cristea, Laura Hinkelman, Karl Lapo, Susan Dickerson, Courtney Moore, Jenna Forsyth, and Alex Fischer for suggestions in the revisions of this manuscript and contributions to fieldwork. Additional contributions to fieldwork were made by Melanie Richmond, Samuel Barr and Jim Syvertsen. I would also like to thank Vince Chaijaroen for access to the University of Washington structural engineering laboratory and help with instrument testing and production as well as Lisa Berman for providing a tree for prototype testing.

John Selker at Oregon State University (Corvallis, Oregon) and Jan Friesen of the Helmholtz Centre for Environmental Research (Leipzig, Germany) are acknowledged for numerous discussions and instrument help.

John Van Stan provided use of the LaserBark system, suggestions, help and equipment for field calibration. He also provided review of data processing techniques and manuscript revisions.

CHAPTER 1: INTRODUCTION

Tree canopy snow interception is a significant hydrologic process which affects the depth and duration of ground snowpack [*Winkler et al.,* 2005]. In highly forested areas, canopy snow interception is the primary control on the amount of snow available for spring melt. During periods of snow accumulation, it has been found that as much as 60% of total snowfall can be intercepted in the canopy [*Hedstrom and Pomeroy*, 1998; *Storck et al.*, 2002]. Once snow is intercepted, it is exposed to ablative processes such as wind and solar radiation and is subject to either sublimation or drip melt. Compounded over an entire season, tree canopy snow interception can account for the removal of up to 40% of water storage from the ground snowpack, when compared to nearby open areas [*Pomeroy and Schmidt,* 1993; *Storck et al.*, 2002; *Jost et al.,* 2007]. This is particularly important in the Pacific Northwest where 80% of land is forested [*USDA Forest Service,* 2000].

In the Western United States, communities rely on the snowpack as a vital water resource, as up to 70% of annual streamflow is provided by snowmelt alone [*Mote et al.*, 2008]. As climate change projections indicate a loss of snowpack and a shift in snowmelt timing to earlier in the season [*Hamlet*, 2011], we must look for ways to optimize the available snowpack depth and duration. Findings from studies on the impacts of forest structure on snowpack suggest that silvicultural manipulation in second-growth forests may help to balance a negative trend in snowpack snow water equivalent (SWE) by reducing the magnitude of snow intercepted by the trees (e.g. *Jost et al.* [2007]). However, in order to fully understand and predict the effects of forest manipulation techniques, we must first be able to accurately quantify snow interception timing and magnitude. Although there have been numerous studies attempting to do so, no one method or model has come forward as the standard.

Several modeling approaches [*Hendrick et al.*, 1971; *Davis et al.*, 1997; *Essery et al.*, 2008] and local-scale empirical studies [*Schmidt and Gluns*, 1991; *Hedstrom and Pomeroy*, 1998; *Lundberg et al.*, 1998] (more empirical studies summarized in a comprehensive review by *Varhola et al*. [2010]) have attempted to represent snow interception timing and magnitude. However, the presence of trees affects the hydrology of a basin through processes which are complex and difficult to predict. Therefore, many models fail to accurately represent snow interception in maritime mountain environments due to the lack of quality field data [*van Heeswijk et al.*, 1996; *Marks et al.*, 1998].

As models and empirical methods have fallen short, many studies have addressed the need for a direct snow interception measurement technique. Despite the large number of existing studies, which have contributed valuable information in an attempt to measure snow canopy interception, no existing technique has been universally implemented. This is likely attributed to the difficulty involved in measuring snow interception for a living tree. Single branch experiments [*Schmidt and Gluns*, 1991; *Bruendl et al.*, 1999] require upscaling estimates from branch to canopy scale and do not represent the entire tree. Whole-cut-tree load experiments [*Nakai et al.*, 1996; *Hedstrom and Pomeroy*, 1998; *Storck et al.*, 2002] and an artificial tree experiment [*Schmidt*, 1991], which removed trees from the stand, are costly, not feasible in a remote environment, and may not represent interception behavior in an undisturbed setting. Gamma-ray attenuation techniques [*Calder and Wright*, 1986] can be costly and require handling of radioactive material. Photograph fractal geometry analysis [*Pomeroy and Schmidt*, 1993] are limited to a small view area, not the entire canopy (for more information, *Lundberg* [1993] provides a comprehensive review of techniques to measure snow interception and evaporation).

Additionally, these existing studies have been largely limited to cold continental climates. Field experiments in maritime climates have been few in numbers with the exception of a cut tree weighing lysimeter experiment [*Storck et al.*, 2002] and a cut tree weighing balance [*Nakai et al.*, 1994]. A robust and simple technique to directly measure snow interception could be implemented in any climatic region or forest structure and would provide a much needed measurement of in situ snow canopy interception.

The instrumentation developed for this study modifies techniques used in the past for tree wind loading [*James and Kane*, 2008] and canopy rain interception [*Friesen et al.*, 2008; *Van Stan II et al.*, submitted]. Unlike rain, which evaporates relatively quickly, the weight from snow interception can be magnitudes greater and can be stored for weeks depending on the amount of snow intercepted, temperature, wind, and presence of liquid precipitation, among other things [*Lundberg et al.*, 1998]. Therefore, a much larger and more persistent compression signal is produced from snow interception when compared to rain interception, which greatly enhances interceptometer signal to noise ratio. To our knowledge, this measurement technique has never been used to quantify snow interception.

This paper presents a relatively inexpensive and non-invasive, in-situ measurement technique to measure snow canopy interception events for living trees, herein referred to as an interceptometer. This technique is applied to quantify tree canopy snow interception and ablation in maritime second growth coniferous forests of the Pacific Northwest. The remainder of this paper seeks to analyze the effectiveness of the interceptometer in its first year of field deployment and shed insight into future use of this technology. The data is also compared to simulated canopy interception as output by the hydrologic Variable Infiltration Capacity (VIC) model [*Liang et al.*, 1994; *Andreadis et al.*, 2009]. This comparison provides a brief analysis of

accumulated interception magnitude and timing. Chapter 2 discusses the theory and background of this technology; Chapter 3 provides a thorough description of the methods used to implement this technology; Chapter 4 summarizes the results of this study. Chapter 5 discusses future implementation of the interceptometer and suggestions for future studies, and Chapter 6 provides concluding remarks.

CHAPTER 2: THEORY AND BACKGROUND

Friesen et al. [2008] demonstrated that any change in canopy mass will result in a measureable trunk compression. This compression can be physically predicted because a tree trunk's behavior closely follows that of a linear elastic material, and can be estimated according to Hooke's law of elasticity. Hooke's law states that the amount a material compresses due to an applied load is proportional to the applied load and measurement length and is inversely proportional to the stiffness of the material, referred to as the modulus of elasticity (MoE), and geometrical properties (Equation 1)

$$\varepsilon_c = \frac{\Delta L}{L} = \frac{P}{AE} \quad (1)$$

where ε_c is the measured trunk compression strain, P is the axial force or weight applied to the trunk, ΔL is the observed sensor displacement, L is the length of the instrumented trunk section (ITS), A is the trunk cross-sectional area, and E is the tree's mean MoE, integrated over the ITS.

The mean modulus of elasticity for softwood green timber can be found readily in timber handbooks. *Green et al.* [1999] reports a mean MoE, for fresh cut softwood timber, of 7.6 GPa. However, the MoE of living wood is sensitive to changes in trunk moisture content, tree trunk diameter, and changes in temperature [*Cannell and Morgan*, 1987]. Therefore, the MoE for each living tree must be individually calibrated [*Friesen et al.*, 2008].

Weight induced trunk displacements (ΔL) tend to be very small. For example, using a weighing lysimeter, *Storck et al.* [2002] found that for an 8 m tall, 2.5 m crown diameter Douglas fir, the maximum snow canopy interception approached 30 mm of SWE over the entire winter. Assuming a 7.6 GPa MoE (as cited above) and a 15 cm trunk radius, we can apply

Equation 1 to calculate a theoretical displacement of about 2.5 μm. Such small displacements may only be captured with sensors capable of extremely high precision. Linear motion potentiometers provide infinite analog resolution [*Bourns*, 2009] allowing for quantification of such small displacements. These displacement sensors are also robust enough to be deployed in a wet and cold environment for an entire winter.

CHAPTER 3: METHODS

3.1 Site description

The study site is located within the Cedar River Municipal Watershed, approximately 50 km east of Seattle, Washington (47° 21' N, 121° 38' W, Figure 3.1a). This area has been classified as the *Tsuga heterophylla* zone, a characteristically wet and mild maritime climate [*Franklin and Dyrness*, 1973]. A western hemlock tree was instrumented with the interceptometer for the 2011/2012 winter.

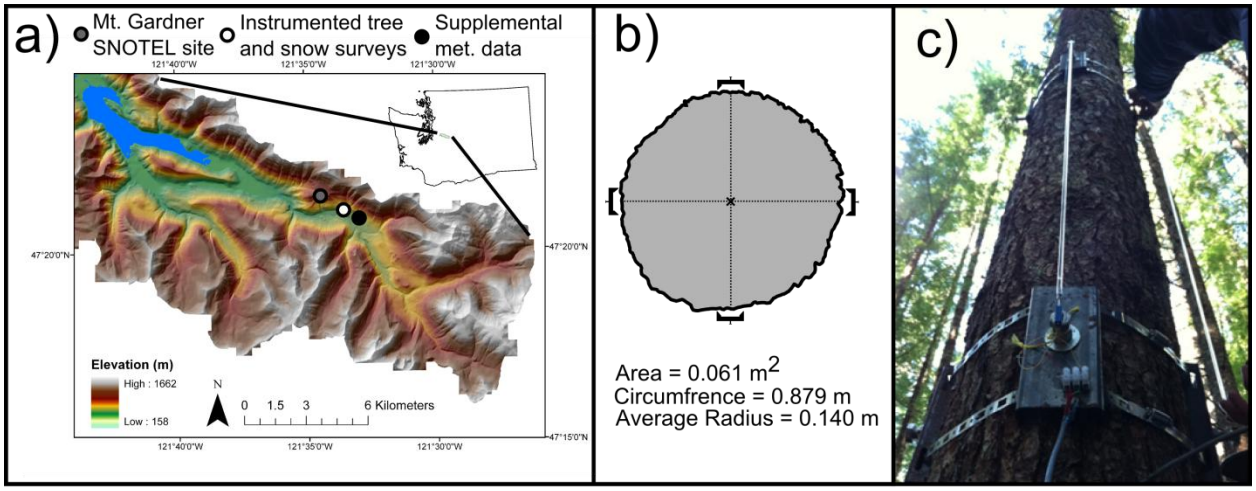

Figure 3.1. a) Map of the study site, b) subject tree cross-section, as measured by the LaserBark, along with computed area, circumference and average radius and c) photo of the installed interceptometer.

The subject tree was located at approximately 640 m elevation on a southwest facing slope of less than 10°. This elevation is within the rain/snow transition zone of the North Cascades, where mid-winter temperatures regularly rise above 0°C. Mean monthly maximum and minimum temperatures at the site are 20.3°C and 8.5°C in July, and 1.9°C and -3.4°C in January. Average annual precipitation is 2,420 mm (1971-2000 climate normals; derived from PRISM, [*Daly et al.*, 2008]). Annual snow accumulation varies between 0 and 2000 mm. Tree species composition in this area is primarily western hemlock (*Tsuga heterophylla*) and Douglas-fir

(*Pseudotsuga menziesii*), although many Western red cedars (*Thuja plicata*) exist. Few silver firs (*Abies alba*) exist at the research site but are predominant at higher elevations in the area. The instrumented trees are representative of the vast majority of trees in the area and are part of a second-growth forest stand of approximately 67 years of age (in 2012), reestablished following clearcut logging in the early 20th century. Second-growth western hemlocks characteristically have tall, slender trunks and a high crown center of mass. The forest canopy at the research site is very dense, and there is generally very little light transmittance to the forest floor (<10% PACL) [*Sprugel et al.*, 2009]. The study sites are situated in a remote location without an external power source or remotely transmitted data capabilities, which is representative of most mountainous environments.

3.2 Snow surveys

Manual snow surveys measuring snow depth and density were conducted in areas of varying canopy cover, described in *Sprugel et al.* [2009]. Open areas were represented by established gaps approximately 60 m (equivalent to the average height of one tree) in diameter, and forested areas were represented by undisturbed, second-growth forest. Approximately 40 snow depth measurements and three snow density measurements were taken in each forest type. During the 2011/2012 winter, eight total snow surveys were conducted, one of which occurred on the 15th of December 2011, shortly after the observation period presented in this paper. Snow depth surveys provide a benchmark on how much snow could potentially be removed by the canopy in forested areas compared to open areas.

3.3 Interceptometer installation

Preceding interceptometer installation, the tree's trunk was scanned using the LaserBark automated tree measurement system [*Van Stan et al.*, 2010] (Figure 3.1b). This technology scans the circumference of the tree, providing a trunk profile, in polar coordinates, with a resolution greater than 10 radii measurements per degree. The geometric center of the trunk is calculated by approximating each successive measurement as a small triangle; once the centroid and area for each individual triangle is found, the centroid and area can be estimated for the entire trunk cross section [*Van Stan et al.*, 2011a]. A laser then marks the exact position of each sensor on the tree, ensuring that the placement is level and evenly distributed about the circumference of each tree. This placement minimizes interceptometer noise and offset from the neutral axes [*Van Stan et al.*, submitted]. Accurate sensor placement is crucial, as sensor misalignment increases error and reduces the signal to noise ratio.

The interceptometer is composed of four linear motion potentiometers, installed on two orthogonal axes which pass through the geometric center of the trunk cross section (Figure 3.1b, 3.1c). The four sensor arrangement allows for measurement redundancy in the event of a failed sensor and estimation verification when using the bending ratio method [*Van Stan et al.*, submitted] method for data processing, further described in Chapter 3.6.1. For the scope of this paper, two methods are demonstrated to isolate tree compression; the strain-diagram method which uses all four of the sensors, and the ratio method, which uses two co-axial sensors. The linear motion potentiometers were extended with 1 m quartz rods in order to achieve a more appreciable displacement measurement. The sensors were glued to brackets which were fixed to the tree using steel banding. Using live computer output, the vertical position of each potentiometer was adjusted until it was centered in the allowable electrical travel range. This

provided the ability to extend or compress as needed in response to wind action or uneven canopy loading. Appendix A provides a full list of parts used and installation procedures.

3.4 Interceptometer data collection

Data in this study were collected using Campbell Scientific CR10X 12-channel, 13-bit data loggers with 2 MB of internal storage. Each of the four interceptometer sensors was sampled in succession with a factory reported delay of 2.6 milliseconds per successive reading [*CR10X Operator's Manual*, 1997]. Data retrieved from the interceptometer were output as changes in millivolts. The raw millivolt signal was converted to a displacement by dividing by the allowable electrical range (2500 mV) and multiplying by the allowable mechanical travel distance (3.81 mm). In an attempt to minimize wind noise and maximize logger storage an interceptometer measurement was taken every second (1 Hz) and the 5-minute average was recorded. This recording scheme was selected to optimize measurement temporal resolution, data logger memory capacity and battery consumption in our remote field sites. Equipment was run off of 12V marine deep cycle batteries. Low winter light and high, dense canopies prevented the use of solar panels. The output interceptometer data were then compared to observed ground SWE accumulation measured with a snow pillow in an area free of forest cover at a nearby NRCS SNOTEL site (Mt. Gardner, marked in Figure 3.1a)

3.5 Potentiometer calibration

Potentiometer calibration was completed using instrumentation provided by the University of Washington structural engineering laboratory. During calibration the potentiometers were subject to 10 known displacements within the range of the potentiometer mechanical travel. These known displacements were then compared to those recorded by the potentiometers' datalogger.

The known and reported displacements were then compared. Individual potentiometer calibration values were determined to be ±1% of factory specifications.

3.6 Data processing to isolated compression signal

Although tree properties can be estimated using assumptions of linear elastic behavior, in reality wood is a slightly nonlinear and heterogeneous material. Additionally, the trunk of a tree is not a perfect cylinder, but instead it tapers and deviates from a straight vertical axis. Trees are naturally structurally slender and are predisposed to bend under axial and in-span loading. This is further complicated by the fact that the tree canopy does not have an even branch/vegetation distribution. Therefore, a snow interception event will not produce a pure compression signal, but rather will be a combination of bending and compression, causing two sensors to compress and two sensors to extend. The compression signal must then be calculated based on the raw bending signal. We employ the bending ratio method (Section 3.6.1) which computes bending ratios using only two of the interceptometer sensors, useful in the event of a failed or suspect sensor and compare this method to a secondary data processing technique using all four interceptometer sensors plotted on a strain diagram (Section 3.6.2).

3.6.1 Bending ratio method

A pure bending test was used to identify the nonlinear bending behavior of each tree and to determine the MoE (Figure 3.2). During this test a neighboring tree was used as an anchor, and a 4:1 pulley system allowed up to 1000 N of tensile force to be established in rope at a height of approximately 5 m above the sensors. By using a simple bending test, the trees can be loaded to both a wide range and large number of bending stresses. Following a successful bending test, the subsequent MoE may also be calculated (see Section 3.7) [*Friesen et al.*, 2008; *James and Kane*,

2008]. Rolling pulleys were utilized at every joint to minimize friction. Bending tests were conducted while the canopy was dry and wind was at a minimum.

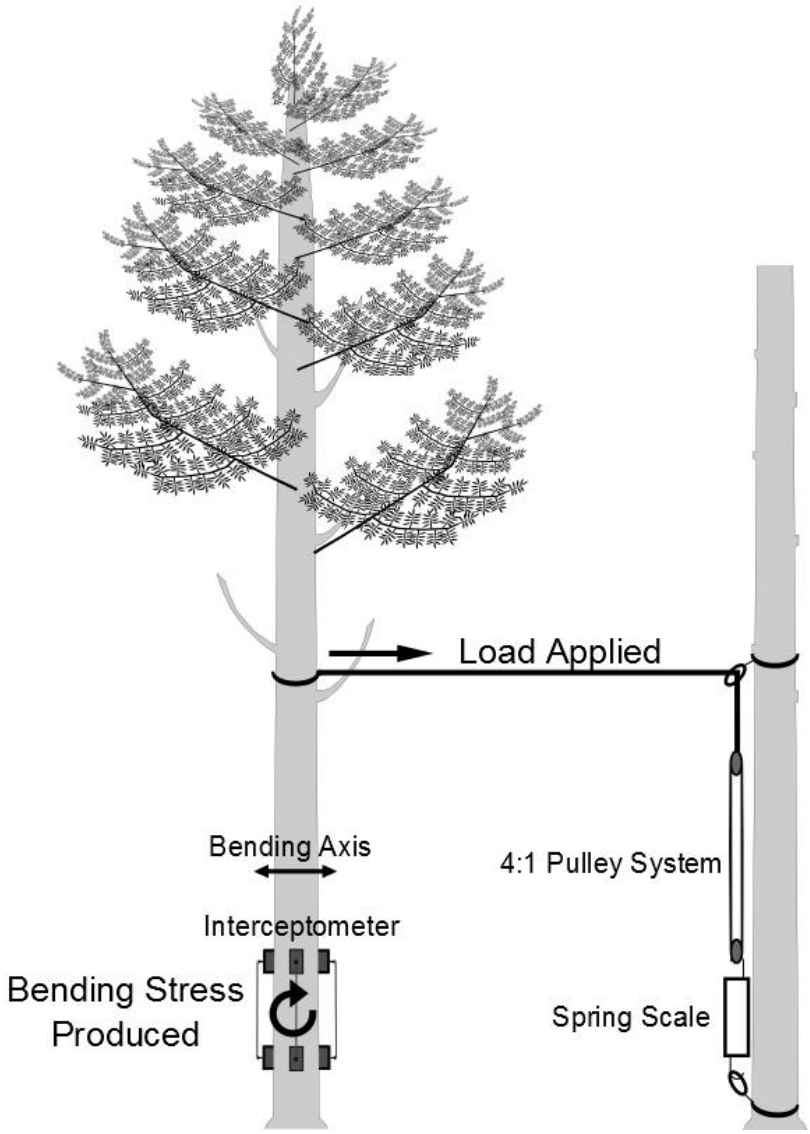

Figure 3.2. A schematic showing the set up for a calibration bending test. Up to 1000 N of tension can be established by tightening the pulley system using a neighboring tree as an anchor. The resulting load can be read directly off the spring scale and the interceptometer records the strain produced. Figure adapted from *Van Stan et al.* [submitted].

During the bending tests it was assumed that no tree canopy loading existed, and all bending was due to the horizontal loads. When bending is applied in line with two of the sensors, one will extend and the other compress; this is referred to as the bending axis (Figure 3.2). In this paper,

sensors going into compression are reported with positive strain and sensors extending are reported as having negative strain. No displacement should be recorded on the two perpendicular sensors, as these sensors lie on what is referred to as the neutral axis. A bending ratio, φ, can then be calculated as the ratio of the displacement between the two opposing sensors which lie on the bending axis (Equation 2).

$$\phi = \frac{\varepsilon_{b1}}{\varepsilon_{b2}} = \frac{\varepsilon_1}{\varepsilon_2} \quad (2)$$

Since there is assumed to be no canopy loading during the bending test, the bending strain will be equivalent to the total strain (Equation 2). In a linear elastic material, with a symmetric cross-section perpendicular to the bending axis, and symmetric potentiometer installation, φ would be -1.0; however as seen in Figure 3.3, φ is computed as -0.96.

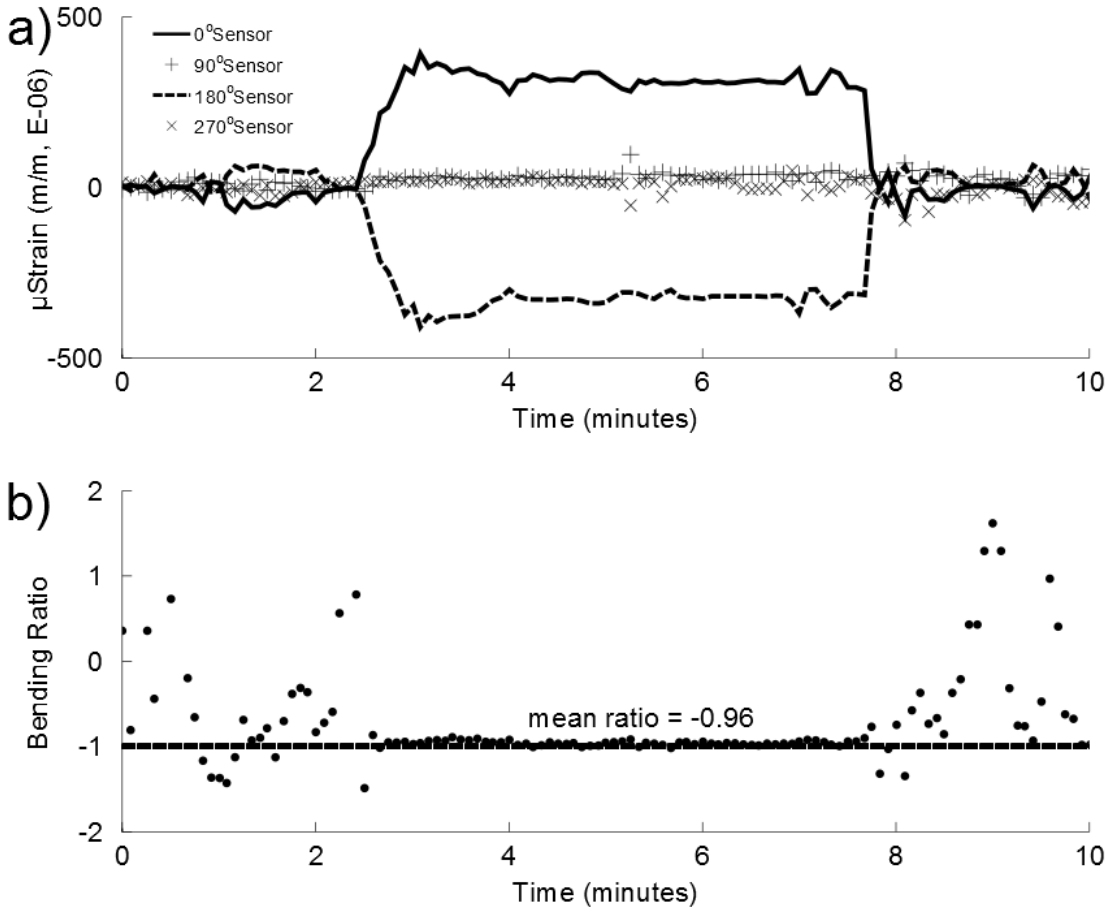

Figure 3.3. Bending data completed 15 June 2012, showing a) significant sensor displacements along the bending axis and virtually no displacement in sensors along the neutral axis and b) mean calculated bending ratio, φ, during testing. A line along φ = -1.0 is drawn to demonstrate ideal bending.

Once the bending ratio is known, it may be applied to interception events to isolate the compression signal. During a snow interception event, the total strain signal in each sensor, ε_i, can be separated into the bending strain, ε_{bi}, and compression strain, ε_c according to Equations 3 and 4.

$$\varepsilon_1 = \varepsilon_c + \varepsilon_{b1} \quad (3)$$

$$\varepsilon_2 = \varepsilon_c + \varepsilon_{b2} \quad (4)$$

Using the bending ratio, the compression strain ε_c can be calculated based on the total strain produced in each sensor during the interception event (Equation 5)

$$\varepsilon_c = \frac{\phi\varepsilon_2 - \varepsilon_1}{\phi - 1} \quad (5)$$

3.6.2 Strain diagram method

As a tree undergoes canopy loading, the entire cross section will experience strain. The interceptometer's four potentiometers, which are distributed orthogonally around the trunk, record the total strain (compression + bending) experienced during a canopy interception event. A strain diagram can be produced by plotting distance from the neutral axis to each individual sensor versus the strain reported for each of the corresponding sensors. While the actual location of the bending neutral axis is not known during an interception event, an optimization scheme is used to find the rotation angle, ϑ, from the neutral axis to each sensor at each time step by maximizing the r-squared value of the line fitting the data when plotted on the strain diagram (Figure 3.4).

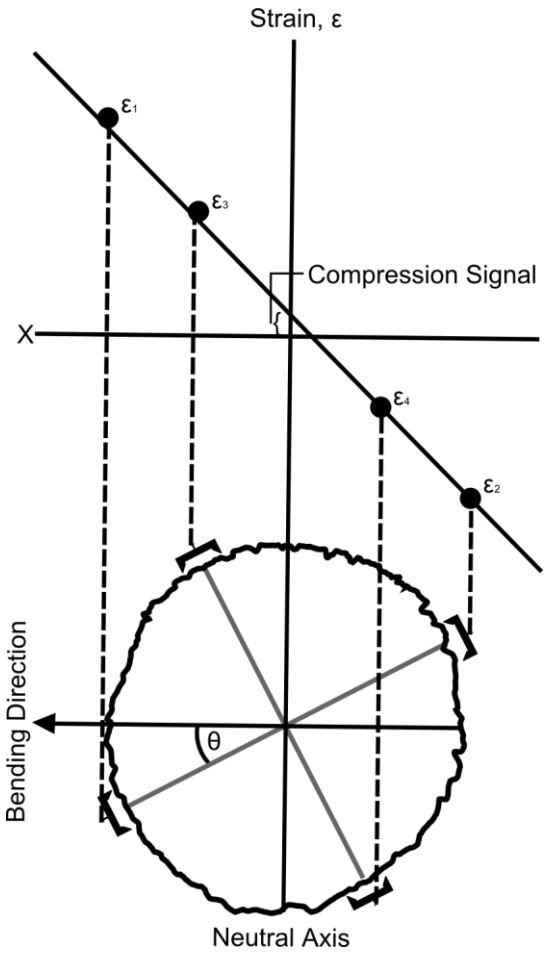

Figure 3.4. A conceptual diagram of the strain diagram method for extracting the compression signal. The distance of the sensor from the neutral axis is plotted versus the total strain recorded by the corresponding sensor. The compression signal is then taken as the y-intercept from the strain diagram.

For the application of the strain diagram method to the November snow event, the optimized r-squared values were all above 0.99. The strain component solely due to compression from the snow loading will be uniform across the trunk's entire cross section. However, due to the presence of bending induced during snow loading, the strain at any point in the trunk's cross section will theoretically be linearly proportional to the perpendicular distance to the bending neutral axis (Figure 3.4). When plotted on the strain diagram, the compression component is taken as the y-intercept.

3.7 Modulus of elasticity

The MoE for a tree is dependent on many things including wood density, water content of the wood [*Green et al.*, 1999; *Cannell and Morgan*, 1987] and wood temperature [*Schmidt and Pomeroy*, 1990]. Because of this variability, the MoE must be calculated for each tree. While loading a tree through a range of bending stresses, the interceptometer will record the resulting bending strains. The data may then be plotted on a stress versus strain curve and the slope of the resulting linear plot is the MoE (Equation 6)

$$E = \frac{\sigma}{\bar{\varepsilon}} \tag{6}$$

where, $\bar{\varepsilon}$ is the average absolute strain of the sensors lying along the bending axis and σ is the bending stress at the outer fiber. For a circular cross section, σ, can be calculated according to Equation 7,

$$\sigma = \frac{My}{\frac{\pi}{32}D^4} \tag{7}$$

where M is the applied moment, y is the distance from the neutral axis to the strain measurement and D is the tree's diameter, measured at the instrumented cross-section.

On 15 June 2012, the trees were incrementally loaded and unloaded using the described bending test. Settling was observed on the spring scale at every loading increment, most likely due to rope stretch and relative movement between the neighboring tree used as an anchor and the subject tree. The results of these bending tests, along with the computed MoE can be seen in Figure 3.5.

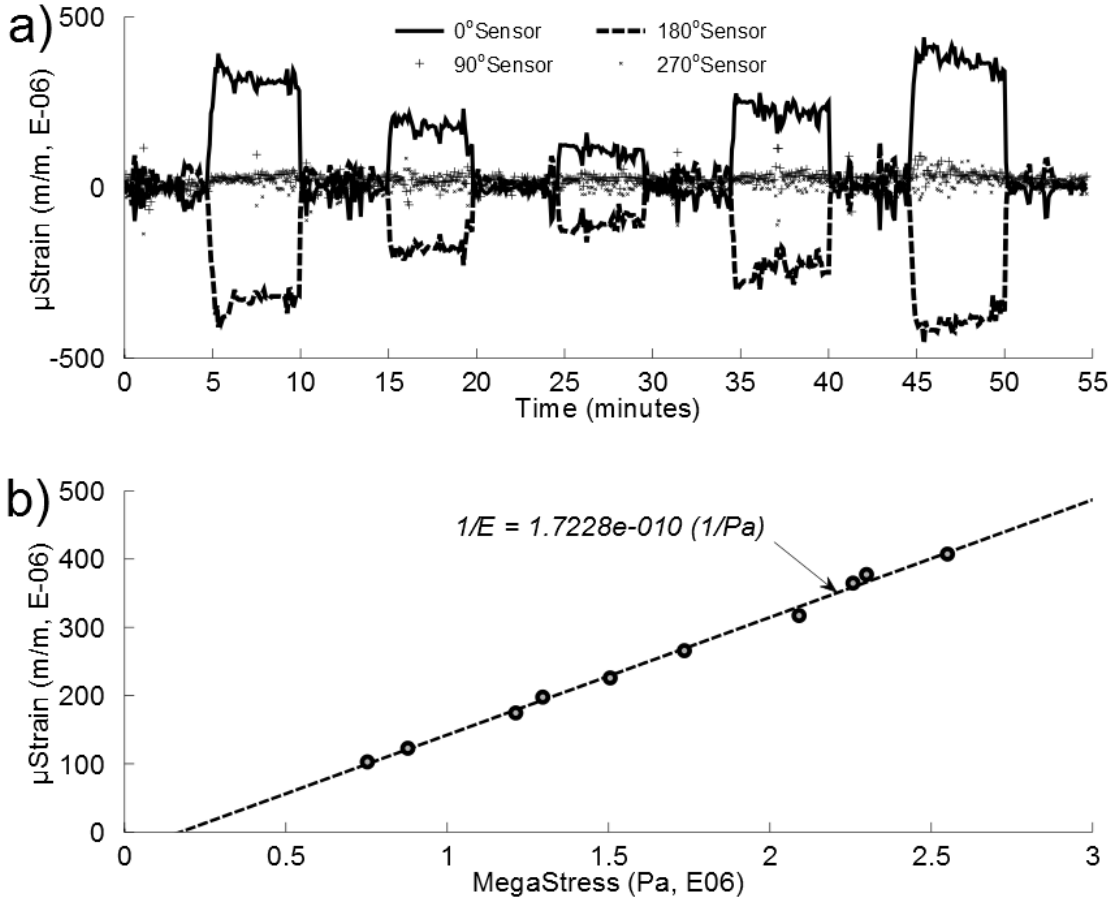

Figure 3.5. Shown above are the a) raw data from a bending test performed 15 June 2012 along a bending axis in-line with the 0° and 180° sensors. The tree was incrementally loaded to different bending stresses, which were read off the spring scale and the strain was recorded by the interceptometer and b) the resulting stress versus strain curve. Where settling on the order of 100 N of tensile force occurred, the bending values were taken as two different points. The MoE, *E*, is calculated as 5.80 GPa.

The MoE was computed as 5.80 GPa which falls within the range reported in various literature for tree species similar to, and including, western hemlock [*Youngs*, 1963; *Cannell and Morgan*, 1987; *Langum et al.*, 2009]. While the actual MoE was likely to have varied during the course of the year, a mid-winter calibration was not feasible. However, the computed SWE is less sensitive to the MoE than the geometric properties of the tree (see sensitivity analysis in Chapter 5.1), which were measured with great accuracy using the LaserBark system.

3.8 SWE calculations

Prior to processing, a second-order, low-pass filter was applied to the raw data to remove any additional noise caused during windy periods. Equation 5 was then applied to the data in order to isolate the pure compression strain, ε_c. Using the compression strain, the weight of the snow in the canopy, *P*, was calculated by rearranging the terms from Hooke's law (Equation 1). Using the weight of snow in the canopy, the equivalent depth of SWE was calculated using the density of water and geometric properties of the tree crown (Equation 8),

$$SWE = \frac{P}{\gamma A_c} \quad (8)$$

where γ is the specific weight of water, 9800 Nm^{-3}, and A_c is the vertically projected crown area, the area of the shadow the crown would make if the sun were directly overhead. The vertically projected crown area was determined by manually staking out the perimeter of the crown using GRS densitometers (www.grs.gis.com). Densitometers provide a cross-hair view directly above the observer. The locations of individual branches were marked on the forest floor, outlining the vertically projected canopy profile. The mean distance from the center of the tree trunk to the furthest reach of the branches was 3.64 m; A_c was then approximated as a circle of area, 45 m^2.

3.9 Modeling

In order to compare observations of snow interception with simulated values, we implemented the Variable Infiltration Capacity (VIC) model for a single grid cell at the location of the experimental plots. The VIC model balances the energy and water budget over a gridded domain based on meteorological and land cover inputs [*Liang, et al.*, 1994; *Cherkauer, et al.*, 2003]. Ground snow accumulation and ablation are represented by a two-layer energy and mass

balance approach, and interception, evaporation, and radiative inputs are modified by vegetation parameters [*Andreadis, et al.*, 2009]. We implemented VIC using estimates of local vegetation characteristics and forced the model with hourly observations of air temperature and wind speed from a meteorological station approximately 1 km from the instrumented tree (Figure 1a) and with disaggregated daily precipitation from the Mount Gardner SNOTEL station, located approximately 2.5 km from the experimental plots, in the Cedar River watershed (Figure 1a). We compared the simulated hourly ground SWE and aggregated intercepted SWE with observations to assess the skill of the model in reproducing the timing and magnitude of interception events recorded by the interceptometer.

CHAPTER 4: RESULTS

The following data are presented for an early winter storm cycle spanning the dates of 10 November to 3 December 2011. Although the interceptometer was deployed for the entire 2011/2012 winter, reoccurring power outages, animal disruptions (elk and black bear) and glue failures affected continuous data collection. Snow surveys conducted during the 2011/2012 winter showed, on average, a 40 cm (60%) greater mid-winter snow depth in open areas as opposed to forested areas suggesting that interception has a strong impact on ground accumulation in forest versus open sites in this area. From a manual snow depth survey conducted on 15 December 2011, an average of 44.2 cm snow depth was reported in the open area compared to an average of 21.8 cm snow depth in the forested area. The average snow density on this day was found to be 0.37 in the open area and 0.33 in the forested area corresponding to a deficit of 91.6 mm SWE (56% of that in the open area) in the forested area following the snow event. Incoming solar radiation remained low, reaching a maximum of 322 W m^{-2} during the storm event (measured at Mount Gardner, Figure 1a).

Snow canopy interception timing and relative shape can be seen for a three week period spanning 11 November to 3 December 2011 from the raw data (Figure 4.1). Relative raw signal and compression magnitudes can be seen by comparing the compression data to the total strain signal. On average, the total strain signal was 17.3 times larger than the processed compression signal. Due to this fact, the processed compression signal can be sensitive to small changes in the overall strain signal. To reduce the compression signal to noise ratio, a low pass data filter removed small noisy patches, likely due to wind signals, in the raw interception signal while maintaining the underlying shape of the data (Figure 4.1).

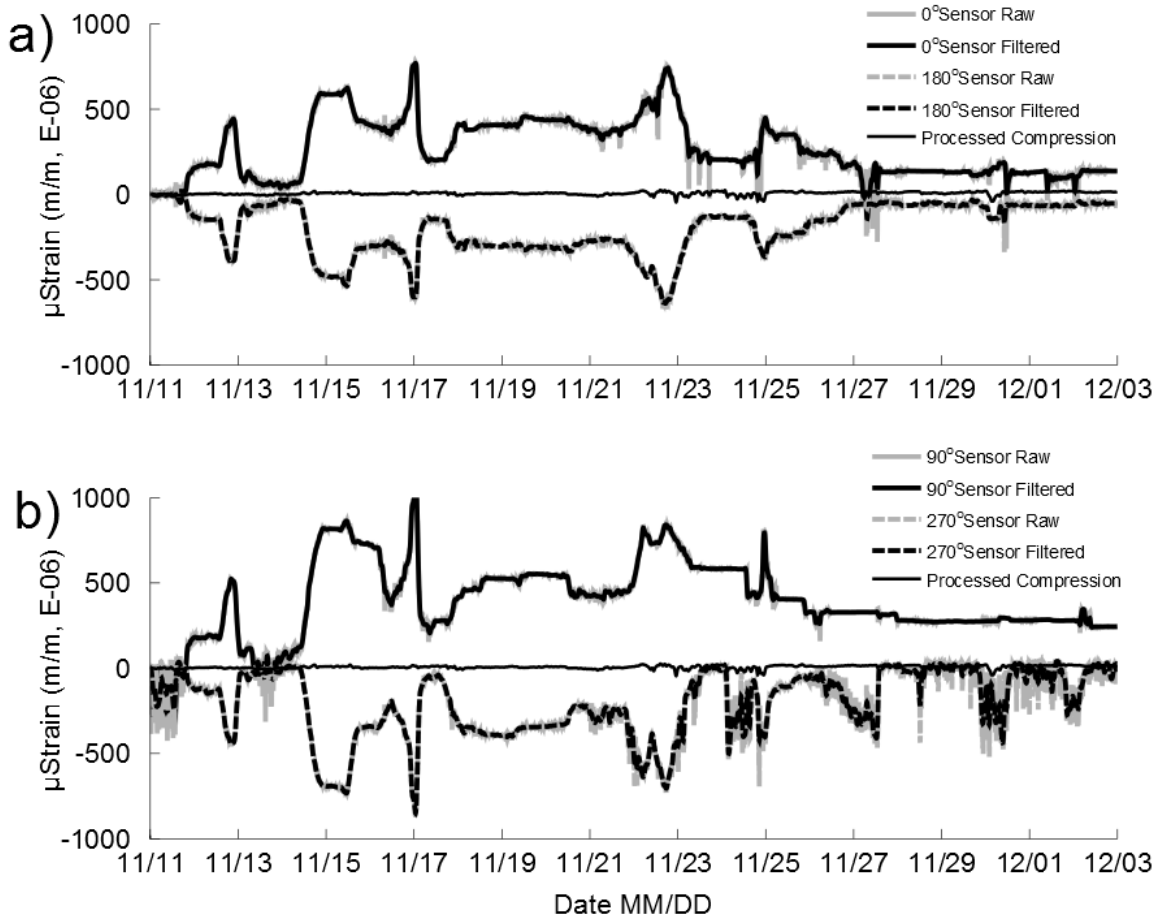

Figure 4.1. Interceptometer raw and filtered strain data along with processed compression data for a) the 0^o to 180^o bending axis and b) the 90^o to 270^o bending axis. Visually it can be seen that the tree is bending somewhere between 0^o and 90^o, but using the strain diagram method we quantified the angle to be 54.7^o. The magnitude of the total strain signal was, on average, 17.3 times larger than the processed compression signal.

The strain diagram method and ratio method were applied to the raw strain signal in order to compute the compression (Figure 4.2a). These two methods had a mean difference of 0.56 mm SWE during the observation period. The two methods had comparable standard deviations, 15.1 mm SWE for the ratio method and 14.0 mm SWE for the strain diagram method. During the observed storm cycle, 180 mm of precipitation fell in the form of snow, measured at the Mount Gardner snow pillow site, the only available SWE data in the area. A snow depth sensor at the supplementary meteorological data station tracked well with the snow depth sensor at Mt.

Gardner (Figure 1a), reporting a mean difference of -6.8 cm snow depth over the course of the observation period. Temperatures routinely rose above 0°C, as is common at the research site, and wind speeds stayed relatively calm, never exceeding 2 m s^{-1} (Figure 4.2b). Although the recordings of zero wind during times with below-zero temperatures are suspicious, near-identical wind patterns were recorded at three surrounding anemometers. If the anemometers were freezing, this was happening uniformly across the study area.

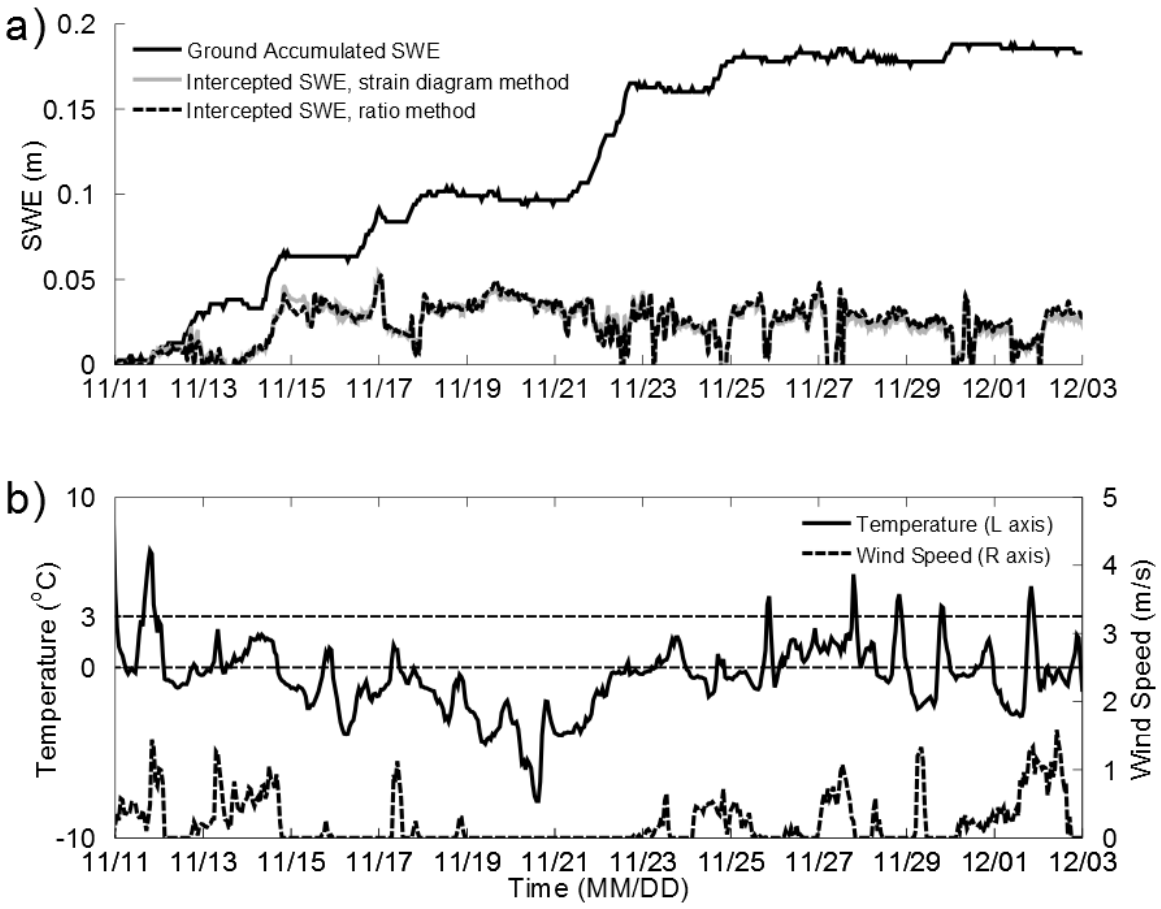

Figure 4.2. Snow canopy interception event showing a) the total accumulated ground SWE and the intercepted SWE as computed by the strain diagram method, the ratio method, and VIC modeled output as well as b) the observed meteorological conditions during the same period, where the horizontal dashed lines represent the 0°C and 3°C thresholds. Although the recordings of zero wind during times with below-zero temperatures are suspicious, near-identical wind patterns were recorded at three surrounding anemometers. If the anemometers were freezing, this was happening uniformly across the study area.

During the early part of the storm cycle, the trees intercepted 83% of total accumulated ground SWE until the canopy reached a maximum carrying capacity of 50.1 mm (Figure 4.3, average of ratio method and strain diagram method). Because snow accumulated and was shed from the canopy in the early part of the storm, Figure 4.3 shows the efficiency for the initial accumulation period and the efficiency for the secondary accumulation period, both in line with the 83% slope.

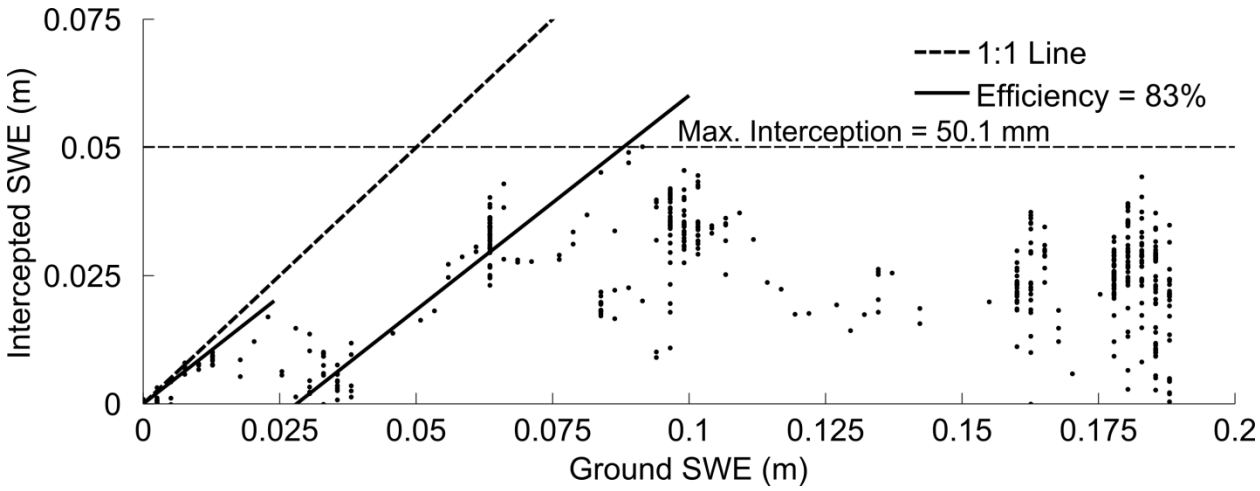

Figure 4.3. Ground SWE measured at the Mt. Gardner SNOTEL station versus intercepted SWE (average of ratio and strain diagram methods) with efficiency lines fit two periods of interception both starting at 0 mm SWE in the canopy.

The VIC model was used to output snow canopy interception using LAI values of 5 and 10 and compared to the measured snow interception using the interceptometer (Figure 4.4). Second-growth western hemlock trees near the study site have been found to have LAI values ranging between 8 and 12. Therefore, the LAI estimate of 10 would be representative of the instrumented western hemlock. By comparing the LAI values of 10 in the model to the LAI value of 5, we gain insight to model behavior and interception dependence on the LAI value. For simplification, model results will be reported for LAI=5(LAI=10). The model reached a maximum interception capacity of 10.0(18.8) mm SWE. Compared to the measured interception, the model

overreported intercepted SWE by 10(17)% for the initial accumulation period and underreported intercepted SWE by 33(16)% for the remainder of the snow accumulation event. The model also failed to represent interception variability such, as canopy accumulation and ablation periods within the storm event, as demonstrated by the low standard deviations of 1.13(3.32) mm SWE when compared to the standard deviations reported by the interceptometer of 15.1 mm SWE as computed by the ratio method and 14.0 mm SWE as computed by the strain diagram method.

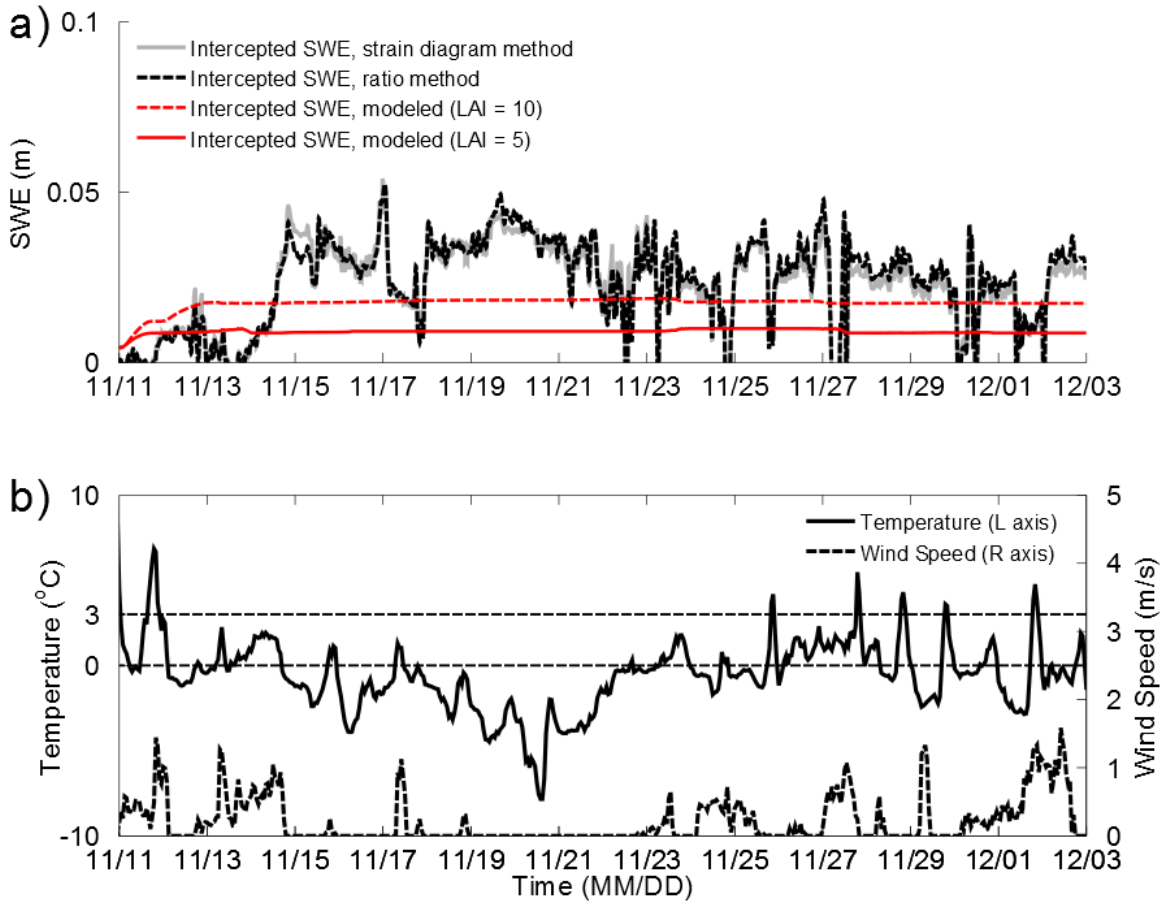

Figure 4.4. a) A direct comparison of the VIC hydrologic model interception output to the measured interception calculated by both the strain diagram method and the ratio method and b) the observed meteorological conditions during the same period, where the horizontal dashed lines represent the 0°C (below which all precipitation falls as snow) and 3°C (above which all precipitation falls as rain) thresholds.

In order to more closely examine the behavior of intercepted canopy SWE over a short time period, a zoomed view of the intercepted SWE is shown in Figure 4.5. During the zoomed period a canopy snow accumulation event and two periods of canopy melt are highlighted. As captured by the snow interceptometer, snow accumulated in the canopy at 3.2 mm hr^{-1} and was shed from the canopy at 0.75 and 0.51 mm hr^{-1}. The model failed to represent these periods of accumulation and ablation. While the canopy accumulation periods, as measured by the interceptometer, correspond to measured snow accumulation at the snow pillow site (Figure 4.5a), the two melt events correspond to only minor increases in temperature and wind speed (Figure 4.5b), signifying that long periods of supporting interception observations would be necessary to train a model to correctly simulate these events.

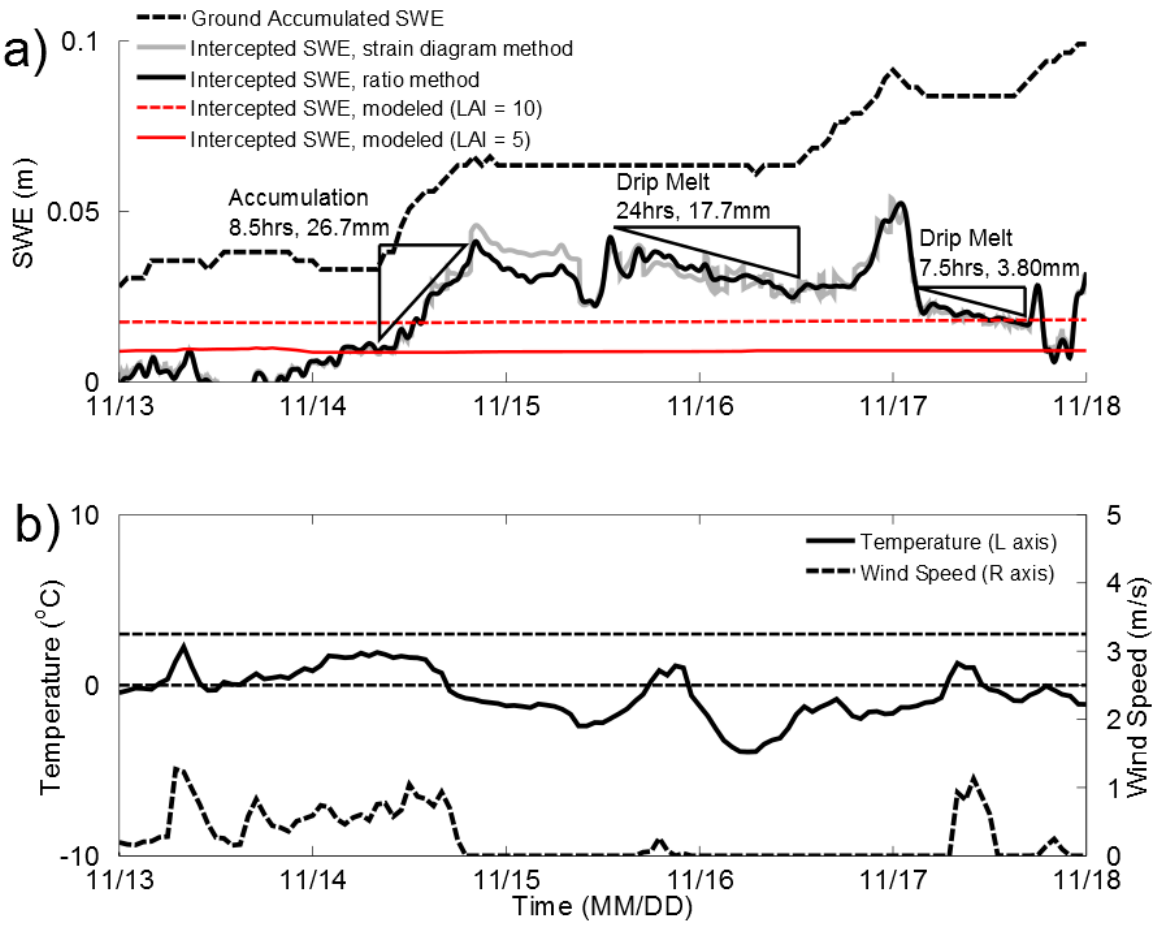

Figure 4.5. A zoomed view, to emphasize periods of accumulation and ablation, of a) the interceptometer SWE signal showing both the ratio method and the strain diagram method compared to the SWE accumulated in a clearing (at the Mount Gardner snow pillow) and b) the observed meteorological conditions during the same period, where the horizontal dashed lines represent the 0°C and 3°C thresholds.

CHAPTER 5: DISCUSSION

5.1 Interceptometer evaluation and sensitivity analysis

Through field calibration, the interceptometer, installed following techniques described in *Van Stan et al.* [2011a], has been shown to lie on perpendicular axes, which minimizes errors resulting from signal processing and enhances the signal to noise ratio (Figure 3.3). Pure bending tests showed a bending ratio of -0.96 along the bending axis and virtually zero displacement along the neutral axis, demonstrating that a tree behaves almost ideally as a linear elastic material at low stress levels (Figure 3.3). The soundness of installation provides confidence in the LaserBark measurement system to identify the geometric center of the tree and estimate the radius and area of the trunk to a high accuracy. The strain diagram method (Figure 3.4) was used in comparison with the bending ratio method to compute the compression signal from the total strain signal and to quantify the bending direction of the tree. The fact that the two methods were within 1% agreement demonstrates the ability to extract the compression signal from the total strain signal using the strain diagram method for four functional sensors, which computes the bending angle, and the ratio method using only two sensors in the event of sensor failure. However, both methods were sensitive to noise in the total strain signal.

While it is unclear what caused unrealistic jumps in the total strain signal in the latter part of the storm, a relatively smooth period void of such jumpy behavior, before 23 November 2011 (Figure 4.2a), demonstrates the potential for high-resolution and accurate interceptometer measurements. During instrument calibration, the interceptometer recorded a linear stress versus strain relationship, which allowed us to calculate the modulus of elasticity of the tree as 5.58 GPa (Figure 3.5). With the exception of branch bending experiments, the modulus of elasticity has

not been previously well quantified for living trees. Due to temperature variation during the winter, the modulus of elasticity may likely have varied throughout the year. A study conducting bending tests throughout the duration of the winter could effectively quantify the variation of the modulus of elasticity, but was beyond the scope of this study. Alternatively, a sensitivity analysis was conducted to quantify the response of intercepted SWE estimate to realistic variations in the modulus of elasticity and errors due to measurement of the projected crown area. Based on previous literature, decreases in temperature increase the modulus of elasticity. For example, changing the temperature from 13^{o}C (maximum temperature on 15 June 2012, date of bending test) to 0^{o}C, corresponds to an increase in MoE of 5% [*Green et al.*, 1999]. Additionally it is feasible that measurement error of the vertically projected canopy area could have been up to 10% as either an over- or under-estimate. By increasing the modulus of elasticity by 5% and decreasing the projected crown area by 10%, we would calculate an average increase in interception efficiency of 15% (for a total efficiency of 98%) and calculated maximum intercepted SWE of 59 mm (a 16.7% increase). By maintaining the calculated modulus of elasticity and increasing the projected crown area by 10%, we would calculate an average decrease in interception efficiency of 7% (for a total efficiency of 76%) and calculated maximum intercepted SWE of 46 mm (a 9.1% decrease).

5.2 Interception comparison to previous literature and model output

Over the entire period of observation the calculated canopy interception showed that our single western hemlock, within a second-growth stand, removed up to 50 mm SWE from the ground snow pack at an efficiency of 83% of snowfall measured in a clearing (Figure 4.3). The sensitivity study conducted provides some insight to what the errors in this estimate could be. The results of a manual snow survey on 15 December 2011, approximately two weeks after the

observation period, shows a 92 mm SWE deficit in the forested area compared to the adjacent open area. While the difference observed in the snow survey could be a combination of interception and melt, they show that it is certainly feasible that the instrumented tree could have intercepted up to 50 mm SWE during the observed period. Additionally, the actual removal of snow from the ground snowpack may be larger for an entire stand than the interception capacity of a single tree, due to the overlapping of tree canopy area in forests increasing interception capacity.

We also ran the VIC hydrologic model for a comparison. While more trees must be instrumented with the interceptometer for more snow events before we can recommend model changes, we can gain some insight from this preliminary study. As shown, the model both underestimated the magnitude of intercepted snow (Figure 4.4), and also failed to capture intrastorm variability (Figure 4.5). Although models are generally run on a large scale and represent considerable forest variability, the results of this study may indicate that the model representation of snow interception behavior could be improved through regional calibration in comparison with direct field measurements of snow canopy interception. To see how the results of this study compare to previous research, we refer to previously cited literature as a comparison of maximum interception capacity and efficiency (Table 5.1)

Table 5.1. Literature review comparing the maximum intercepted canopy SWE (mm) and the efficiency, reported as a percentage of total accumulated snowfall, for various tree types and geographic locations. A direct measurement is a measure of whole canopy tree interception, while indirect indicates an estimation technique for determining whole canopy interception.

Study	Method	Location	Tree Species	Maximum Interception mm SWE (efficiency)
Bunnell et al., [1985]	Direct, tree weighing apparatus	British Columbia, Canada	Douglas fir	30 (45%)
Calder, [1990]	Direct, tree weighing apparatus	Scotland	Sitka spruce	30 (66%)
Johnson, [1990]	Indirect, precipitation - (throughfall + stemflow)	Scotland	Sitka spruce	22 (28%)
Schmidt, [1991]	Direct, tree weighing apparatus	Colorado, USA	artificial conifer	N/A (58%)
Schmidt and Gluns, [1991]	Indirect, cut branch experiment	Colorado, USA and British Columbia, Canada	Engleman's spruce	N/A (50%)
			lodgepole pine	N/A (45%)
			subalpine fir	N/A (45%)
Pomeroy and Schmidt, [1993]	Indirect, manual snow surveys	Saskatchewan, Canada	black spruce	3.5 (60%)
			jack pine	7 (45%)
Nakai, [1996]	Direct, tree weighing apparatus	Sapporo, Japan	6 conifer species	30 (50%)
Hedstrom and Pomeroy, [1998]	Indirect, paired under-canopy and open-area snow gauges	Saskatchewan, Canada	jack pine	N/A (30%)
			black spruce	N/A (45%)
Storck et al., [2002]	Direct, tree weighing lysimeter	Oregon, USA	Douglas fir	40 (60%)
This Study	**Direct, tree interceptometer**	**Washington, USA**	**western hemlock**	**50 (83%)**

As seen in Table 5.1, the results of the present study show both a larger interception magnitude and efficiency than previous studies. Many of the previously cited studies are in cold, continental climates. In continental climates trees often have thinner canopies when compared to trees in maritime climates and the snow that falls is often less dense due to lower temperatures and may slough off the branches more easily. However, this study also reports higher interception magnitude and efficiency that studies in comparable maritime climates. This may be due to a difference in tree type and behavior. The trees in dense second-growth stands battle for

light and as a result, have very high and dense canopies which may be capable of intercepting more snow than an isolated tree. Furthermore, as noted at our field site, the canopies tend to bridge which may allow for a higher interception capacity where the tree canopies overlap.

5.3 Recommendations for future installations

Although the interceptometer was disrupted several times during the 2011/2012 winter, this study provided a prototype-level installation. Therefore, future implementations of this technology could gain considerably from where our instruments failed. During the course of the winter, we noted several opportunities for improving upon the instrument installation presented here.

The data collection system used in this study represents the lower end of the available technological spectrum. Increases in data storage capacity, datalogger resolution, and battery usage efficiency will only improve instrument performance. During this application, the data was sampled at a high frequency (1 Hz) and the 5-minute average was recorded in an attempt to maintain a high sample rate and optimize datalogger storage space. We were able to utilize this recording scheme due to the persistence of snow in the canopy. An application of the interceptometer to record wind throw or rain interception would require a higher sampling rate and resolution and would not allow for averaging.

A bracket design which is not strapped to the tree trunk, but drilled directly into the tree could ease significantly ease installation processes. An improved bracket design would allow for slight rotations about the x- and y-axes as well as translations in the z-direction. The ability for slight adjustments during installation would ensure that the instrument would be aligned both vertically and horizontally, eliminating torque where the quartz rod meets the potentiometer. By

reducing the number of connections in the interceptometer, it would reduce the number of places where glue has the potential to fail. During the installation glue failure occurred on several instances. Finding a reliable glue and, as mentioned, reducing the number of connections would lessen the probability of glue failure.

The implementation of a track-and-hold circuit would allow for near instantaneous measurement of all four sensors in the potentiometer. The datalogger specifications for our installation report a 2.3 millisecond delay in successive sampling. This delay could produce errors due to displacements caused by wind while the interceptometer is being sampled. We employed a high frequency measurement technique, while taking a longer term average. However a track-and-hold circuit would allow for a higher sampling frequency and the assurance of eliminating error as a result of sampling delay.

Through further instrument testing and development, a more robust and simpler design could be achieved allowing for significant improvements in instrument performance. The interceptometer may then also not only improve our understanding of canopy interception, however it may have applications for research beyond snow interception. The interceptometer could also be used to gain information regarding trees which pose hazard to buildings and power lines, through observations of wind, and loading during ice storms. By identifying actual loading, models could be developed for failure criteria, and suspect trees could be removed avoiding potentially catastrophic destruction.

5.4 Broader Implications

This study has demonstrated that the interceptometer is capable of measuring the canopy intercepted SWE for an individual tree. The development of the snow interceptometer represents

a new technique to quantify snow canopy interception. Since the interceptometer is installed in situ on a single tree within a stand, the recorded interception behavior is representative of how trees behave in their natural environment. Due to the non-destructive installation methods, the interceptometer may be ideal for observations in environmentally sensitive areas such as old-growth forest stands. The relative ease of interceptometer installation could allow for examining the interception behavior of a larger sample size of trees. By sampling more trees, subsequent studies could effectively capture variation in interception behavior due to trees of different age and species, as well as trees of varying elevation, slope, aspect, and stand type and climatic regions. This type of variation has not previously been represented and would provide data essential for model validation and training. By improving model representation of interception, watershed managers interested in the effects of silvicultural manipulation to optimize snowpack, could examine the effects of removing trees on the watershed scale.

CHAPTER 6: CONCLUSIONS

The results of this study represent the successful deployment of the tree interceptometer to record snow canopy interception. Using the *Van Stan et al.* [2011a] method for interceptometer installation we have demonstrated even sensor spacing and achievement of the neutral axis. The interceptometer is a technology which can be installed relatively easily and inexpensively, in live trees within existing canopy structures in any watershed. Where models may fail to represent interception efficiency, maximum interception capacity, and intrastorm interception variability, the interceptometer serves as a practical method for model validation and regional calibration. While the quantification of tree canopy interception has previously been difficult to attain, the tree interceptometer may be a viable tool to increase the number of interception studies in any region, remote or accessible. By sampling more trees, subsequent studies could effectively capture variation in interception behavior due to trees of different age and species, as well as trees of varying elevation, slope, aspect, and stand type and climatic regions. With this information watershed managers may then plan for silvicultural manipulation in specific areas to optimize the amount of water stored in the ground snowpack for spring melt.

REFERENCES

Alig, R.J, D. Zheng, T.A. Spies, and B.J. Butler (2000), Forest cover dynamics in the Pacific Northwest west side: Regional trends and projections, *USDA Forest Service Research Paper, PNW-RP-522*.

Andreadis, K.M., P. Storck, and D.P. Lettenmaier (2009), Modeling snow accumulation and ablation processes in forested environments. *Water Res. Res., 45*, 1-13.

Bourns (2009), 3046 linear motion potentiometer. http://www.bourns.com/pdfs/3046.pdf

Bründl M., P. Bartelt, M. Schneebeli, and H. Flühler (1999), Measuring branch deflection of spruce branches caused by intercepted snow load. *Hydrol. Proc., 13*, 2357-2369.

Calder, I.R. and I.R. Wright (1986), Gamma ray attenuation studies of interception from Sitka spruce: Some evidence for an additional transport mechanism, *Water Res. Res., 22*(3), 409-417.

Cannell, M.G.R., and J. Morgan (1987), Young's modulus of sections of living branches and tree trunks. *Tree Physiology, 3*, 355-364.

Cherkauer, K.A., L.C. Bowling, and D.P. Lettenmaier (2003), Variable infiltration capacity cold land process model updates. *Global and Planetary Change, 38*, 151-159.

CR10X measurement and control module operator's manual (1997), Campbell Scientific, Inc.

Daly, C., M. Halbleib, J.I. Smith, W.P. Gibson, M.K. Doggett, G.H. Taylor, J. Curtis, and P.A. Pasteris (2008), Physiographically-sensitive mapping of temperature and precipitation across the conterminous United States. *Int. J. Climatol., 28*, 2031-2064.

Davis, R., J. Hardy, W. Ni, C., Woodcock, J. McKenzie, R. Jordan, and X. Li (1997), Variation of snow cover ablation in the boreal forest: a sensitivity study on the effects of conifer canopy. *J. Geophys. Res., 102*, 29389-29395.

Essery, R., P. Bunting, J. Hardy, T. Link, D. Marks, R. Melloh, J. Pomeroy, A. Rowlands, N. Rutter (2008), Radiative transfer modeling of a coniferous canopy characterized by airborne remote sensing. *J. Hydrometeorol., 9*, 228-241.

Franklin, J. F., and C. T. Dyrness (1973), Natural vegetation of Oregon and Washington. Oregon State University Press, Corvallis, 464 p.

Friesen, J., C. van Beek, J. Selker, H. H. G. Savenije, and N. van de Giesen (2008), Tree rainfall interception measured by stem compression, *Water Resour. Res., 44*, W00D15, doi:10.1029/2008WR007074.

Green, D.W., J.E. Winandy, D.E. Kretschmann (1999), Mechanical properties of wood. Wood handbook : wood as an engineering material. Madison, WI : USDA Forest Service, Forest Products Laboratory, General technical report FPL, GTR-113: 4.1-4.45.

Green, D.W., J.W Evans, J.D. Logan, and W.J. Nelson (1999), Adjusting modulus of elasticity of lumber for changes in temperature, *Forest Prod. J., 49*(10), 82-94.

Hamlet, A. F. (2011), Assessing water resources adaptive capacity to climate change impacts in the Pacific Northwest Region of North America. *Hydrology and Earth System Sciences, 15*(5), 1427-1443. doi:10.5194/hess-15-1427-2011.

Hedstrom, N. R., and J. W. Pomeroy (1998), Measurement and modelling of snow interception in the boreal forest, *Hydrol. Processes*, *12*, 1611 –1625.

Hendrick, R.L., B.D. Filgate, and W.M. Adams (1971), Application of environment analysis to watershed snowmelt. *J. Appl. Meteorol., 10,* 418-429.

James, K. R., and B. Kane (2008), Precision digital instruments to measure dynamic wind loads on trees during storms, *Agric. Meteorol., 148*(6–7), 1055– 1061, doi:10.1016/j.agrformet.2008.02.003.

Jost, G., M. Weiler, D. Gluns, and Y. Alila (2007). The influence of forest and topography on snow accumulation and melt at the watershed-scale. *J. Hydrol., 347,* 101–115.

Langum, C.E., V. Yadama, and E.C. Lowell (2009). Physical and mechanical properties of young-growth Douglas-fir and western hemlock from western Washington. *Forest Prod. J., 59*(11/12), 37-47.

Liang, X., D.P. Lettenmaier, E.F. Wood, and S.J. Burges, 1994. A simple hydrologically based model of land surface water and energy fluxes for general circulation models. *J. of Geophys. Res., 99,* 14415-14428.

Lundberg, A. (1993), Evaporation of intercepted snow—Review of exisiting and new measurement methods, *J. Hydrol., 151,* 267–290.

Lundberg, A., I. Calder, and R. Harding (1998), Evaporation of intercepted snow: Measurement and modeling, *J. Hydrol., 206,* 151–163.

Marks, D., J. Kimball, D. Tingey, and T. Link (1998), The sensitivity of snowmelt processes to climate conditions and forest cover during rain-on-snow: A case study of the 1996 Pacific Northwest flood, *Hydrol. Processes*, *12*, 1569– 1587.

Mote, P., A. Hamlet, and E. Salathe (2008), Has spring snowpack declined in the Washington Cascades?, *Hydrol. Earth Syst. Sci., 12,* 193-206.

Nakai, Y., T. Sakamoto, and T. Terajima (1994), Snow interception by forest canopies; weighing a conifer tree, meteorological observation and analysis by the Penman-Monteith formula, *Snow and Ice Covers: Interactions with the Atmosphere Ecosystems* (Proceedings of Yokohama Symposia J2 and J5, July 1993).

Nakai, Y. (1996), An observational study on evaporation from intercepted snow on forest canopies, Doctoral Thesis, Department of Agriculture, Kyoto University, Kyoto Japan, 107 pp.

Pomeroy, J.W., and R.A. Schmidt (1993), The use of fractal geometry in modeling intercepted snow accumulation and sublimation. Proceedings of the 50th Eastern Snow Conference, Quebec City, 1-10.

Schmidt, R.A. (1991), Sublimation of snow intercepted by an artificial conifer, *Agric. For. Meteorol.*, *54*, 1-27.

Schmidt, R. A., and D. R. Gluns (1991), Snowfall interception on branches of three conifer species, *Can. J. For. Res.*, *21*, 1262– 1269.

Schmidt, R.A., and J.W. Pomeroy (1990), Bending of a conifer branch at subfreezing temperatures: implications for snow interception. *Can. J. For. Res.*, *20*, 1250-1252.

Sprugel, D.G., K.G. Rascher, R. Gersonde, M. Dovčiak, J.A. Lutz, and C.B. Halpern (2009), Spatially explicit modeling of overstory manipulations in young forests: Effects on stand structure and light. *Ecological Modeling*, *220*, 3565-3575.

Storck, P. (2000), Trees, snow and flooding: An investigation of forest canopy effects on snow accumulation and melt at the plot and watershed scales in the Pacific Northwest. *Water Resources Series*, *161*.

Storck, P., D.P. Lettenmaier, and S.M. Bolton (2002), Measurement of snow interception and canopy effects on snow accumulation and melt in a mountainous maritime climate, Oregon, United States, *Water Resour. Res.*, *38*(11), 1223, doi:10.1029/2002WR001281.

Van Heeswijk, M., J. Kimball, and D. Marks (1996), Simulation of water available for runoff in clearcut forest openings during rain-on-snow events in the western Cascade Range of Oregon and Washington, *U.S. Geol. Surv. Water Resour. Invest. Rep.*, 95-4219, 67.

Van Stan, J.T., M.T. Jarvis, and D.F. Levia (2010), An automated instrument for the measurement of bark microrelief, *IEEE Trans. Instr. Measure.*, *59*, 491-493.

Van Stan, J.T., M.T. Jarvis, D.F. Levia, and J. Friesen (2011a), Instrumental method for reducing error in compression-derived measurements of rainfall interception for individual trees, *Hydrol. Sci. J.*, *56*, 1061-1066.

Van Stan, J.T., K.A. Martin, J. Friesen, M.T. Jarvis, J.D. Lundquist, and D.F. Levia (submitted), Evaluation of an instrumental method to reduce error in canopy water storage estimates via mechanical displacement, Submitted to *Water Resour. Res.*

Varhola A, N.C. Coops, and M. Weiler (2010), Forest canopy effects on snow accumulation and ablation: an integrated review of empirical results, *J. Hydrolometerol.*, *33*, 392-219.

Winkler, R.D., D.L. Spittlehouse, and D.L. Golding (2005), Measured differences in snow accumulation and melt among clearcut, juvenile, and mature forests in southern British Columbia. *Hydrol. Proc.*, *19*, 51–62.

Youngs, R.L. (1963), Strength and related properties of mountain hemlock, *US Forest Service Research Paper*, *FPL 3*.

APPENDIX A

Full list of interceptometer parts:

(1) Bourns model 3046L 0.15 in (3.81 mm) electrical travel linear motion potentiometers acted to output the change in length of the ITS.

(2) Size 0-80 hex nuts were screwed to the threaded end of the potentiometer slide bar to increase gluing surface area,

(3) 5 mm diameter, 1m long quartz tubing acted to extend the measurement length of the potentiometers, to achieve a more appreciable measurement.

(4) Brackets (3x6") machined from 3x3x.125" square steel tubing with ½-13 bolts centered on the face allowed the potentiometers and tubing to be anchored to the tree trunk.

(5) Arc magnets (polarized through the radius) were glued to the bolt head at the bracket as well as to the potentiometer/tubing, when these pieces were brought together a free axis of rotation was created ensuring no torque was placed on the potentiometers.